Gallium(III) Catecholate Complexes as Probes for the Kinetics and Mechanism of Inversion and Isomerization of Siderophore Complexes[1]

Berthold Kersting, Jason R. Telford, Michel Meyer, and Kenneth N. Raymond*

Contribution from the Department of Chemistry, University of California, Berkeley, California 94720

Received October 23, 1995[⊗]

Abstract: The catechol siderophore analog $K_3[Ga(\mathbf{3})_3]$, **4** ($H_2\mathbf{3}$ = 2,3-dihydroxy-*N*,*N*′-diisopropylterephthalamide), is D_3-symmetric in aqueous solution, and exists in two enantiomeric forms, Δ-**4** and Λ-**4**. Variable temperature NMR experiments demonstrate that the inversion of the enantiomers of **4** in D_2O is facile. The rate of inversion is independent of pH above pH 8. The mechanism is intramolecular. From line-shape analysis the free energy of activation $\Delta G^{\ddagger}_{298}$ = 67.4(9) kJ mol^{-1} in D_2O at pD 12.1, with $\Delta H^{\ddagger}$ = 58.5(6) kJ mol^{-1} and $\Delta S^{\ddagger}$ = −0.030(9) kJ mol^{-1} K^{-1}. Below pD 8 the rate of inversion for **4** is pD dependent and initially first order in [D^+]. Potentiometric titrations reveal that **4** protonates in two one-proton steps with log K_{HML_3} = 4.66(4) and log $K_{H_2ML_3}$ = 3.99(7). In DMSO-d_6, formation of a tight contact ion pair between K^+ and $[Ga(\mathbf{3})_3]^{3-}$ ions increases the free energy barrier to inversion by ∼7 kJ mol^{-1}. The complex $K_3[Ga(\mathbf{9})_3]$, **10** ($H_2\mathbf{9}$ = 2,3-dihydroxy-*N*-*tert*-butyl-*N*′-benzylterephthalamide), was prepared to elucidate the mechanism of inversion by dynamic NMR spectroscopy, using the fact that **10** exists in two isomeric forms, *cis*-**10** and *trans*-**10**, which are of C_3 and C_1 symmetry in solution. The ratio *cis*-**10**:*trans*-**10** is 0.78(3) at ambient temperature in D_2O or DMSO-d_6. Two processes are distinguishable on the NMR time scale in D_2O or DMSO-d_6, *cis*-**10**−*trans*-**10** isomerization and the inversion of the enantiomers of *trans*-**10**. Both processes proceed intramolecularly with T_c = 295(1) K for Λ-*trans*-**10** to Δ-*trans*-**10** inversion and T_c = 335(1) K for *cis*-**10** to *trans*-**10** isomerization in D_2O at pD 9.5. The discrete exchange pattern of the *tert*-butyl resonances during inversion of *trans*-**10** confirms that the reaction proceeds by a trigonal twist mechanism *via* a trigonal prismatic transition state. The free energy barriers to inversion are $\Delta G^{\ddagger}_{295}$ = 60 kJ mol^{-1} in D_2O (pD 9.8) and $\Delta G^{\ddagger}_{327}$ = 67 kJ mol^{-1} in DMSO-d_6.

Introduction

Siderophore-mediated iron uptake in microorganisms is generally stereospecific.[2−6] In general, the pseudooctahedral metal centers of these complexes are chiral and are differentially recognized by chirally-specific membrane-bound protein receptors. In the absence of direct structural data, the mechanism of recognition by these membrane-bound receptors has been inferred from substrate mapping.[2,3] The importance of the metal complex configuration to recognition has generally been derived from uptake or inhibition studies of kinetically-inert complexes formed by replacing the labile, high-spin ferric ion with kinetically inert metal ion substitutes.[5,6]

Enterobactin, composed of a cyclic triester of serine in which the three amino groups are conjugated to 2,3-dihydroxybenzoic acid units to form a tricatechol ligand, is important because of its wide-spread utilization by bacterial pathogens. It forms a 1:1 ferric complex with an absolute configuration at the metal center that is Δ.[7] Some time ago it was shown that the synthetic, mirror image enterobactin (which consequently has Λ configuration at the metal center) does not promote growth, as does the natural siderophore.[8] It was presumed that this was because of stereospecific recognition at the outer membrane of ferric enterobactin by the receptor protein. Subsequently it has been found that the mirror image compound enantioenterobactin is nearly as efficient in promoting transport across the outer membrane as is the natural enterobactin.[9] Where the mirror image compound differs from enterobactin is at the culmination of the iron transport step, transport across the cytoplasmic membrane, and release of iron associated with enterobactin hydrolysis. Is the rate of inversion of configuration at the metal center of such a complex fast enough to affect these recognition and transport processes? While the three catechol units of enterobactin are tethered, the high stability of tricatecholate complexes at medium to high pH makes metal−ligand dissociative processes unlikely for such inversion and isomerization. Hence, simple tricatecholate complexes provide a useful model in determining the minimal rate, and probable mechanism, associated with the isomerization reaction leading to inversion at the metal center.

* To whom corrrespondence should be addressed.

⊗ Abstract published in *Advance ACS Abstracts,* June 1, 1996.

(1) Coordination Chemistry of Microbial Iron Transport. 59. Part 58: Hou, Z; Sunderland, C. J.; Nishio, T.; Raymond, K. N. *J. Am. Chem. Soc.* **1996**, *118*, 5148.

(2) Ecker, D. J.; Loomis, L. D.; Cass, M. E.; Raymond, K. N. *J. Am. Chem. Soc.* **1988,** *110*, 2457.

(3) Matzanke, B. F.; Müller-Matzanke, G.; Raymond, K. N. Iron Carriers and Iron Proteins. In *Physical Bioinorganic Chemistry Series*; Loehr, T. M., Ed.; VCH Publishers: New York, 1989; pp 1−121.

(4) *CRC Handbook of Microbial Iron Chelates;* Winkelmann, G., Ed.; CRC Press: Boca Raton, FL, 1991.

(5) Raymond, K. N.; Telford, J. R. Siderophore-mediated Iron Transport in Microbes. In *Bioinorganic Chemistry An Inorganic Perspective of Life;* Kessissoglou, D. P., Ed.; NATO ASI Series; Kluwer Academic Publishers: Dordrecht, The Netherlands, 1995; Vol. 459, pp 25−37.

(6) Raymond, K. N.; Müller, G.; Matzanke, B. F. *Top. Curr. Chem.* **1984**, *123*, 49.

(7) Karpishin, T. B.; Dewey, T. M.; Raymond, K. N. *J. Am. Chem. Soc.* **1993**, *115*, 1842.

(8) Venuti, M. C.; Rastetter, W. H.; Neilands, J. B. *J. Med. Chem.* **1979**, *22*, 123.

(9) Nishio, T.; Bryan, B.; Raymond, K. N. Manuscript in preparation.

S0002-7863(95)03545-1 CCC: $12.00

Analyses of the rearrangement reactions of tris-bidentate complexes have occupied an important part of the development of coordination chemistry.[10−13] A concerted twist motion of the chelates about a trigonal face of the octahedron, without disconnecting a metal−ligand bond, generates a trigonal-prismatic transition state. When this is around the trigonal face that corresponds to the 3-fold axis of the D_3 point symmetry of a symmetrical trichelate, the Bailar twist results.[14] Evidence for inversion reactions proceeding via this trigonal-prismatic transition state has been obtained in a few complexes in which the bidentate ligand is small. In these systems, it has been concluded that the trigonal twist mechanism may be favored by ground-state distortions toward the transition state.[15] An analysis of isomerization and inversion reactions of trischelate complexes of siderophore-type ligands has not appeared in the literature, although a sterically constrained macrobicyclic tricatecholatoiron(III) complex has been shown to have a trigonal-prismatic coordination geometry.[16]

The major limitation to the study of such reactions in iron−siderophore type complexes is their kinetic lability. This prevents the separation of isomerically and enantiomerically pure compounds and studies under nonequilibrium conditions.[17] In addition, the large line widths and accompanying poor spectral resolution of high-spin Fe(III) complexes tend to rule out dynamic NMR studies of isomerization. However, gallium(III), because of its similar chemistry,[18,19] can be used instead of iron, and the reactions at chemical equilibrium can be investigated by NMR spectroscopy. Similar protocols have been employed to characterize the kinetics and mechanism of inversion of tris(acetylacetonate) and tritropolonate complexes of various metal ions in nonaqueous solvents.[20−23] In the present study, variable temperature ^{1}H NMR spectroscopic studies have been employed to investigate the kinetics and mechanism of inversion and isomerization reactions of these diamagnetic gallium(III) complexes of synthetic siderophore-type ligands in aqueous solution. A combination of pD-dependent NMR spectra and potentiometric titration was carried out to characterize these reactions over a broad pH range. The complexes were also studied in aprotic solvents. Finally, the corresponding iron(III) complexes were prepared and their structures in solution investigated by infrared and vis/UV spectroscopy.

Results and Discussion

Syntheses. The ligands used in this study, H_2**3** and H_2**9**, were synthesized according to Schemes 1 and 2. Gallium(III) and iron(III) complexes of H_2**3** and H_2**9** were obtained by the reaction of the respective monopotassium salts K[H(**3**)] and K[H(**9**)] with $Ga(acac)_3$ or $Fe(acac)_3$ in CH_3OH at room temperature. The complexes $K_3[M(L)_3]$ (L = **3**, M = Ga, **4**; M = Fe, **5**; L = **9**, M = Ga, **10**; M = Fe, **11**) were obtained in high yields and were purified by recrystallization. The anions $[Ga(\mathbf{3})_3]^{3-}$ and $[Fe(\mathbf{3})_3]^{3-}$ were also isolated as tetramethylammonium salts **12** and **13**. All complexes decompose upon prolonged exposure to air, and the potassium salts are quite hygroscopic.[24] Positive ion fast-atom-bombardment mass spectra showed the molecular ion peaks of the mononuclear 1:3 complexes. The isotope distribution patterns are consistent with mononuclear metal complexes. Two stereoisomers are possible for **10** (*cis*-**10** and *trans*-**10**), and ^{1}H NMR spectroscopy of **10** in DMSO-d_6, CD_3OD, or D_2O displays two sets of proton resonances, corresponding to these isomers. At 295 K integration of the *tert*-butyl signals indicates the *cis* to *trans* ratio for **10** in DMSO-d_6 is 0.78(1).

Scheme 1

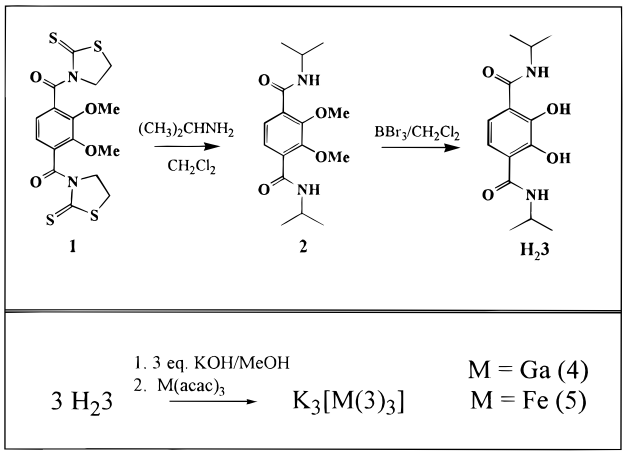

Scheme 2

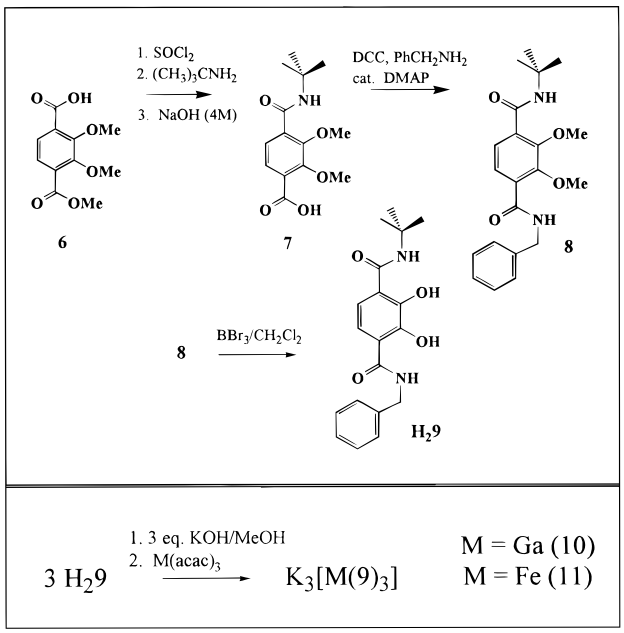

IR and Vis/UV Spectroscopy. IR spectral data of the ligands H_2**3** and H_2**9** showed strong absorptions in the regions 3450−3350 and 1600−1550 cm^{-1}, corresponding to NH and CO stretching modes, respectively.[25] Upon coordination to gallium-

(10) (a) Basolo, F.; Pearson, R. G. *Mechanisms of Inorganic Reactions*, 2nd ed.; Wiley: New York, 1967. (b) Wilkins, R. G. *Kinetics and Mechanism of Reactions of Transition Metal Complexes*, 2nd ed.; VCH Publishers: New York, 1991.
(11) Fay, R. C.; Piper, T. S. *Inorg. Chem.* **1964**, *3*, 348.
(12) Fortman, J. J.; Sievers, R. E. *Inorg. Chem.* **1967**, *6*, 852.
(13) Gordon II, J. G.; Holm, R. H. *J. Am. Chem. Soc.* **1970**, *92*, 5319.
(14) Bailar, Jr, J. C. *J. Inorg. Nucl. Chem.* **1958**, *8*, 165.
(15) Rodger, A.; Johnson, B. F. G. *Inorg. Chem.* **1988**, *27*, 3062.
(16) Garrett, T. M.; McMurry, T. J.; Hosseini, M. W.; Reyes, Z. E.; Hahn, F. E.; Raymond, K. N. *J. Am. Chem. Soc.* **1991**, *113*, 2965.
(17) McArdle, J. V.; Sofen, S. R.; Cooper, S. R.; Raymond, K. N. *Inorg. Chem.* **1978**, *17*, 3075.
(18) Borgias, B. A.; Barclay, S. J.; Raymond, K. N. *J. Coord. Chem.* **1986**, *15*, 109.
(19) Loomis, L. D.; Raymond, K. N. *J. Coord. Chem.* **1991**, *23*, 361.
(20) Eaton, S. S.; Holm, R. H. *J. Am. Chem. Soc.* **1971**, *93*, 4913.
(21) Hutchison, J. R.; Gordon, J. G., II; Holm, R. H. *Inorg. Chem.* **1971**, *10*, 1004.
(22) Eaton, S. S.; Hutchison, J. R.; Holm, R. H.; Muetterties, E. L. *J. Am. Chem. Soc.* **1972**, *94*, 6411.
(23) Eaton, S. S.; Eaton, G. R.; Holm, R. H.; Muetterties, E. L. *J. Am. Chem. Soc.* **1973**, *95*, 1116.

(24) Gemlike crystals of **4**, **5**, **12**, and **13** were easily grown by ether diffusion in alcoholic solutions of the metal complexes. However, all of the diffraction patterns obtained from rotation photographs showed diffuse reflections.

Table 1. ^{1}H NMR Data for H_2**3**, K_3[Ga(**3**)$_3$], and [NMe_4]$_3$[Ga(**3**)$_3$] in CD_3OD and DMSO-d_6[a]

H_2**3**		K_3[Ga(**3**)$_3$]		[NMe_4]$_3$[Ga(**3**)$_3$]		
CD_3OD	DMSO-d_6	CD_3OD	DMSO-d_6	CD_3OD	DMSO-d_6	assignment
n.o.	8.60 (d)	n.o.	10.76 (d)	n.o.	10.75 (d)	N*H*CO
7.30 (s)	7.35 (s)	6.98 (s)	6.65 (s)	6.96 (s)	6.67 (s)	Ar*H*
4.22 (spt)	4.14 (oct)[b]	4.03 (spt)	3.84 (oct)[b]	4.03 (spt)	3.85 (oct)[b]	C*H*(CH_3)$_2$
				2.95 (s)	3.03 (s)	N(CH_3)$_4^+$
1.24 (d)	1.18 (d)	1.19 (d)	1.09 (d)	1.22 (d)	1.10 (d)	CH(CH_3)$_2$
		1.01 (d)	0.95 (d)	1.05 (d)	0.97 (d)	CH(CH_3)$_2$

[a] Chemical shifts are in ppm with respect to Me_4Si (0.0 ppm) at 298 K; s = singlet, d = doublet, sep = septet, oct = octet. Coupling constants are included in the Experimental Section. [b] NH/ND exchange in DMSO is slow on the NMR time scale; the similar coupling constants ($^3J_{NHCH} \approx {}^3J_{CHCH}$) cause overlapping of the two septets to yield an octet for the methine proton.

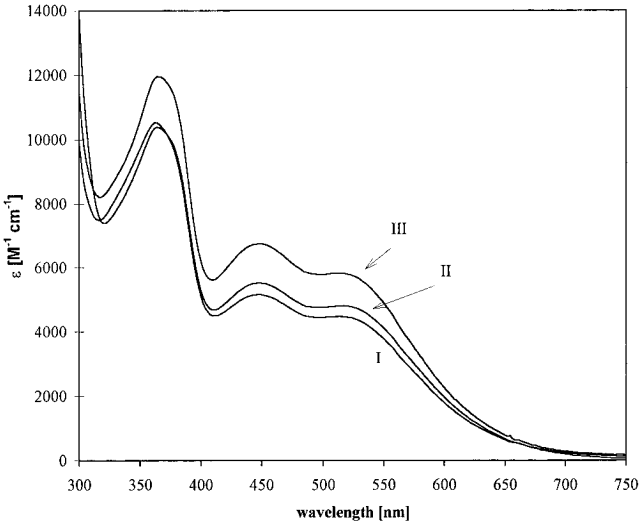

Figure 1. Electronic absorption spectra of **5** (I) (5.4×10^{-5} M), **11** (II) (4.9×10^{-5} M), and **13** (III) (4.3×10^{-5} M) in H_2O (5% KH_2PO_4, pH 9.1).

(III) or iron(III), a slight shift to higher wavenumbers in the CO stretching modes was observed, while the lower absorption of the two NH modes was shifted by 150 cm^{-1} in the opposite direction. Both NH bands are also significantly broadened. These effects are indicative of intramolecular hydrogen bonding between the NH protons and ortho catecholate oxygen atoms in the metal complexes. This conclusion is supported by the ^{1}H NMR data of the gallium complexes in DMSO-d_6 solution (*vide infra*).

As shown in Figure 1, the absorption spectra of **5**, **11**, and **13** in H_2O at pH 9.1 are very similar. Intense absorptions (>4000 M^{-1} cm^{-1}) appear in the UV due to ligand to metal charge transfer (LMCT) and ligand-localized $\pi-\pi^*$ electronic transitions.[26] The absorption bands at ~364 nm are readily assigned as $\pi-\pi^*$ transitions of the ligands, while the bands at 446 and 510 nm are assigned as LMCT transitions. The energy and intensity of the bands are typical for octahedral or pseudooctahedral tris(2,3-dihydroxyterephthalamide)-iron(III) complexes. By comparison, because of a higher degree of π-bonding in related trigonal-prismatic iron(III) complexes, a shift of the higher energy LMCT to 428 nm is observed.[16,26]

NMR Spectral Data for $H_2$3, 4, and 12. The ^{1}H and ^{13}C NMR data for H_2**3**, K_3[Ga(**3**)$_3$], and (NMe_4)$_3$[Ga(**3**)$_3$] are presented in Table 1. Upon complexation of Ga^{3+} by **3**, the amide protons are shifted from 8.60 ppm observed in the free ligand to 10.76 ppm, indicative of intramolecular hydrogen bonding of the amide protons and ortho catecholate oxygen atoms.[27] ^{1}H NMR spectra of the [Ga(**3**)$_3$]$^{3-}$ anion in D_2O, CD_3OD, or DMSO-d_6 are all very similar, the only major difference being the absence of the NH resonance in protic solvents due to rapid NH/ND exchange. The ring, methine, and methyl proton resonances of the metal complexes are shifted upfield when compared to those of the free ligand. The methyl proton resonances of the isopropyl group, which appear as a singlet in the spectrum of the free ligand, are inequivalent and together with the methine proton form an A_3B_3X system. Correspondingly two signals, one for each inequivalent methyl carbon atom, are observed in the ^{13}C NMR spectrum of **4**. Relative to the protonated free ligand, the largest shifts are observed for the carbon atoms bonded to the catecholate oxygens. The other resonances are only slightly shifted. It is also clear that the choice of counter cation does not influence the NMR properties of the [Ga(**3**)$_3$]$^{3-}$ anion. On the basis of these data the structure of the [Ga(**3**)$_3$]$^{3-}$ complex anion in solution is assigned D_3 symmetry, with the three 2,3-dihydroxyterephthalamide ligands chelated to gallium. The same symmetry has been observed for closely related complexes of gallium(III) in the solid state.[28] The complex **4** is chiral and forms the racemate of the two enantiomeric forms **Λ-4** and **Δ-4.** The interconversion of both enantiomers would result in a site exchange of the two inequivalent methyl proton resonances. This dynamic process was analyzed by variable temperature ^{1}H NMR spectroscopy.

Kinetics of Inversion for 4. At 295 K, **4** displays an A_3B_3X pattern for the methyl and methine protons and two ^{13}C resonances for the methyl groups of the isopropyl residues in DMSO-d_6 or CD_3OD. The methyl proton and carbon resonances result from geminal methyl groups, which are diastereotopic because **4** is dissymmetric (the complex is chiral, point group D_3).

In D_2O, the A_3B_3X pattern of **4** is observed only above pD 8 and the A_3B_3 part of the A_3B_3X system coalesces on warming or on lowering pD. Variable temperature ^{1}H NMR spectra of **4** in D_2O were collected in phosphate-buffered solutions at pD 7.2, 9.8, and 12.1. A set of selected spectra of **4** at pD 9.8 (methyl proton region) is shown in Figure 2. Coalescence is observed at $T_c = 330$ K, and further heating results in a single doublet for the methyl protons. No significant change in coalescence temperature is observed when the pD is raised to 12.1 (332 K). However, at pD 7.2 coalescence already occurs at 288 K.

The observed coalescence of the methyl group protons is due to inversion of configuration of **4**. Line-shape analysis of the experimental spectra afforded the respective calculated spectra and rate constants (see Figure 2). The rate constants were fitted as a function of $1/T$ according to the Arrhenius ($k = A \exp(-$

(25) *Spectroscopic Techniques For Organic Chemists*; Cooper, J. W., Ed.; John-Wiley & Sons: New York, 1980.
(26) Karpishin, T. B.; Gebhard, M. S.; Solomon, E. I.; Raymond, K. N. *J. Am. Chem. Soc.* **1991**, *113*, 2977.
(27) Albrecht, M.; Franklin, S. J.; Raymond, K. N. *Inorg. Chem.* **1994**, *33*, 5785.
(28) Karpishin, T. B.; Stack, T. D. P.; Raymond, K. N. *J. Am. Chem. Soc.* **1993**, *115*, 6115.

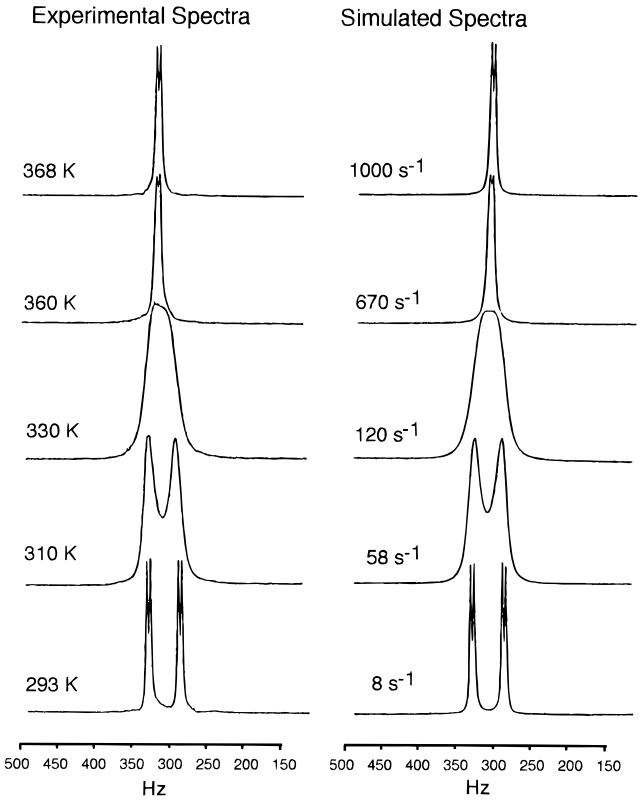

Figure 2. Variable temperature ^{1}H NMR spectra of **4**, 0.015 M, in D_2O at pD 9.8. Experimental spectra (left column) and simulated spectra (right column) of methyl proton resonances in the temperature range 293−370 K.

E_a/RT)) and Eyring ($k = (k_BT/h)\exp(-\Delta G^{\ddagger}/RT)$) equations to obtain the values of E_a, log A, $\Delta G^{\ddagger}$, $\Delta H^{\ddagger}$, and $\Delta S^{\ddagger}$. The kinetic parameters derived from these fits are reported in Table 2.

Analysis of the data shows that in D_2O the inversion of configuration of **4** is proton independent over the range of pD where the $[Ga(\mathbf{3})_3]^{3-}$ complex is stable (pD > 8, *vide infra*). For example, values of the activation energy, E_a, for inversion of configuration change only slightly from 57.7(4) kJ mol^{-1} at pD 9.8 to 61.2(5) kJ mol^{-1} at pD 12.1.

Evidence for an intramolecular mechanism for the Λ-**4** ↔ Δ-**4** interconversion is provided by the ^{1}H NMR spectra of **4** in the presence of H_2**3**, at pD 9.8. The methyl proton resonances of H_2**3** would coalesce with the resonances of **4** if the process were intermolecular. However, even at temperatures above the coalescence temperature, the observed spectra consist of resonances corresponding to the complex and the free ligand (see Figure 3). Furthermore, as expected for first-order kinetics, the rate constants are independent of concentration. A quantitative study with three different concentrations (0.015, 0.030, and 0.045 M) at pD 9.8 and 12.1 afforded no change in k at 25 °C or T_c, which remain unchanged within experimental error.

Intramolecular inversion of configuration should show little or no solvent effects on T_c. Accordingly, when D_2O was replaced with DMSO-d_6, the coalescence temperature was found to be 360 K, corresponding to an increase in $\Delta G^{\ddagger}$ of 7 kJ mol^{-1}.[29] A similar increase in $\Delta G^{\ddagger}$ was observed in an analogous variable temperature ^{1}H NMR study for **10** (*vide infra*). We note that **4** is freely soluble in D_2O but only slightly soluble in DMSO-d_6, where it probably exists as a tight contact ion pair.[30] In D_2O the potassium cations are solvated and separated from the anion. Accordingly a slight cation dependence on the free energy barrier to inversion is expected for **4** in DMSO-d_6.

pD Dependence of Inversion for 4. The ambient temperature ^{1}H NMR spectrum of **4** in D_2O at pD 7.2 showed coalescence with T_c = 288 K. This behavior prompted the examination of the pD dependence of the rate of inversion for **4**. From pD 8.5 to about pD 6.2, the evolution of the ^{1}H NMR spectrum of **4** was similar to that shown in Figure 2. The rate constants at T = 298 K calculated for each pD value by lineshape analysis are plotted versus pD in Figure 4. Below pD 8 the rate of inversion for **4** is dependent on, and initially first order in, [D$^+$]. A determination of the solution thermodynamics of **4** proceeded on the assumption that the effect is due to a different species, which is in equilibrium with **4** at low pD. Refinement of potentiometric titration data yielded two one-proton steps. The corresponding protonation constants are log K_{MHL_3} = 4.66(4) and log $K_{MH_2L_3}$ = 3.99(7). Figure 5 displays a species distribution plot calculated for **4** in D_2O as a function of pH. From pH 7 the species $[GaH(\mathbf{3})]^{2-}$ is in equilibrium with $[Ga(\mathbf{3})_3]^{3-}$, and its concentration increases to approximately 5% at pH 6. Protonation of $[GaH_2(\mathbf{3})]^-$ results in dissociation of the complex to give the free ligand, which precipitates. This behavior can be compared and contrasted with similar complexes of iron(III)[31] and gallium(III).[19,32] While the kinetically active species may not be the same as the thermodynamic species, the rate of inversion for **4** can be described as a function of pD by taking into account the sequential protonation:

$$\text{rate} = k_0[Ga(L)_3{}^{3-}] + k_1[GaD(L)_3{}^{2-}] + k_2[GaD_2(L)_3{}^{-}]$$

where the rate constants correspond to the rate of inversion of each of the complex species in the equation. In the pD range studied (6.2−12) a diprotonated species does not contribute to the rate. Hence, the rate expression can be written as

$$\text{rate} = k[Ga(L)_3{}^{3-}] \quad \text{where} \quad k = k_0 + k_1[D^+]$$

The rate constants k_0 and k_1 were fit to the data by a weighted nonlinear least-squares method ($w_i = 1/k_i^2$), to give k_0 = 9.0(6) s^{-1} and $k_1 = 6.4(2) \times 10^9$ M^{-1} s^{-1}. The equilibrium structural changes which occur on equilibrium protonation of tris(2,3-dihydroxyterephthalamide) complexes have been investigated in detail for iron(III) and gallium(III), and are associated with linkage isomerism. The complexes rearrange intramolecularly to a salicylate mode of coordination in which one phenolate oxygen of the Ga complex is protonated and replaced by the adjacent amide carbonyl oxygen.[33,34] However, the salicylate complex which is the thermodynamic product of the protonation reaction must itself result from a bond breaking process that (presumably) follows protonation of the coordinated catechol oxygen atom. Hence, it likely follows, rather than being the

(29) The rate constant k_c, (s^{-1}), calculated from the equation $k_c = 2.22\delta$, at the coalescence temperature is 126 s^{-1} in D_2O (δ = 57 Hz) and 92 s^{-1} in DMSO-d_6 (δ = 41 Hz) for the inversion of configuration of (Δ,Λ)-**4**. The free energy barrier to inversion (kJ mol^{-1}) was calculated from the equation $\Delta G^{\ddagger} = 19.13 \times 10^{-3}T_c(9.97 + \log(T_c/k_c))$. This approximation yielded $\Delta G^{\ddagger}$ = 67 kJ mol^{-1} in D_2O and $\Delta G^{\ddagger}$ = 74 kJ mol^{-1} in DMSO-d_6. The former value is in good agreement with the value obtained from the full line-shape analysis.

(30) A similar, weakly polar interaction involving Me_4N^+ cations was observed in the crystal structure of a related gallium(III) complex with tris-(2,3-dihydroxyterephthalamide) coordination. Stack, T. D. P.; Karpishin, T. B.; Raymond, K. N. *J. Am. Chem. Soc.* **1992**, *114*, 1512.

(31) Garrett, T. M.; Miller, P. W.; Raymond, K. N. *Inorg. Chem.* **1989**, *28*, 128.

(32) Pecoraro, V. L.; Wong, G. B.; Raymond, K. N. *Inorg. Chem.* **1982**, *21*, 2209.

(33) Cass, M. E.; Garrett, T. M.; Raymond, K. N. *J. Am. Chem. Soc.* **1989**, *111*, 1677.

(34) Loomis, L. D.; Hahn, F. E.; Raymond, K. N. Unpublished results.

Table 2. Kinetic Parameters for the Inversion of $K_3[Ga(\mathbf{3})_3]$ in D_2O and DMSO-d_6[a]

solvent[b]	$\Delta G^{\ddagger}_{298}$ (kJ mol^{-1})	$\Delta H^{\ddagger}$ (kJ mol^{-1})	$\Delta S^{\ddagger}$ (kJ mol^{-1} K^{-1})	E_a (kJ mol^{-1})	log A	k_{298} (s^{-1})
D_2O (pD 7.2)	60(3)	46(2)	−0.047(5)	48(2)	10.8(3)	240(10)
D_2O (pD 9.8)	66.8(6)	55.2(3)	−0.039(9)	57.7(4)	11.2(1)	11(1)
D_2O (pD 12.1)	67.4(9)	58.5(6)	−0.030(9)	61.2(5)	11.7(1)	10(1)
DMSO	73(2)	67(1)	−0.02(1)	70(2)	12.1(2)	4(1)
DMSO[c]	75(2)	77(1)	0.00(1)	80(2)	13.5(3)	1(1)

[a] Arrhenius and Eyring activation parameters were obtained from the least-squares fit of log k vs $1/T$ and log(k/T) vs $1/T$ plots, respectively. All errors (in parentheses) are random errors estimated at the 95% confidence level. [b] Concentration 0.015 M; the D_2O solutions are phosphate buffered. [c] The NMe_4^+ salt.

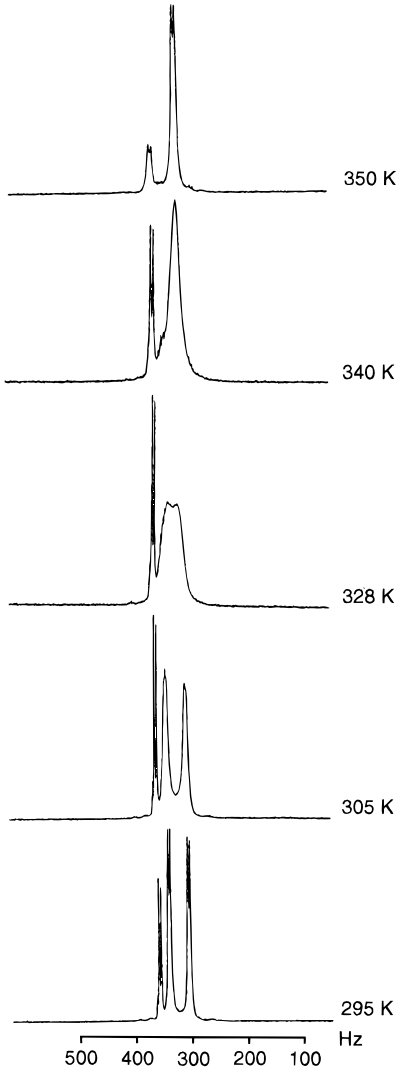

Figure 3. Variable temperature ^{1}H NMR spectra of a mixture of H_2**3** and **4**, 0.015 M, in D_2O at pD 9.8 (temperature range 295−350 K). Experimental spectra of methyl proton resonances.

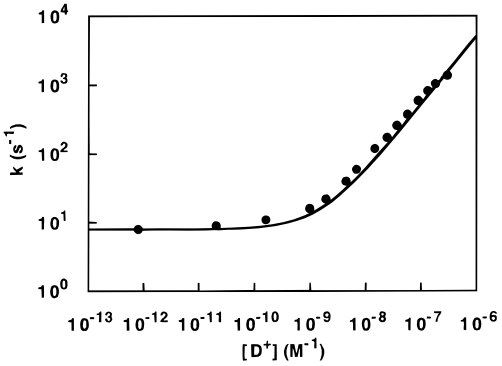

Figure 4. pD dependence of the rate constants for the interconversion of the enantiomers of **4** in D_2O (circles). Rate constants were obtained by line-shape analysis of the experimental spectra (isopropyl methyl proton region) recorded in buffered D_2O solutions at 298 K (5% phosphate buffer; [**4**] = 0.015 M). The rate constants were fit to the equation $k = k_0 + k_1[D^+]$ by least-squares methods (k_0 = 9.0(6) s^{-1}, k_1 = 6.4(2) × 10^9 M^{-1} s^{-1}).

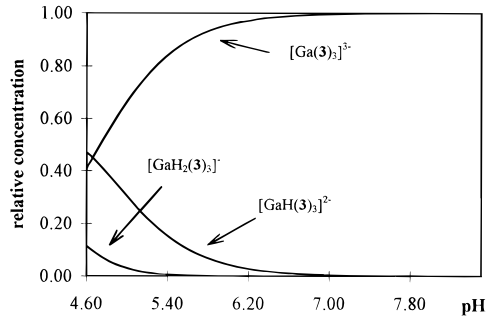

Figure 5. Species distribution plot calculated for **4** in H_2O as a function of pH at T = 298 K. [**4**] = 0.015 M.

rate-determining step of, the inversion reaction for the $[GaHL_3^{2-}]$ species. Until the mechanism of the catecholate−salicylate interchange is also determined, this will not be certain, but it seems likely that in the protonated intermediate the gallium remains coordinated by six phenolate oxygen atoms, one of which has been protonated.

Isomerization and Inversion in 10. The preceding section established that inversion of the $[Ga(\mathbf{3})_3]^{3-}$ complex proceeds by an intramolecular mechanism. Several pathways for this type of rearrangement exist, which cannot be distinguished from the study of complexes like **4**, in which the ligand **3** is a symmetric bidentate ligand. In contrast, the kinetics of isomerization and inversion reactions of the *cis* and *trans* isomers of trischelate complexes of the type $[M(L)_3]^{3-}$ in which L is an asymmetrical bidentate ligand can distinguish the different intramolecular rearrangements.[10]

An example of such a complex is $K_3[Ga(\mathbf{9})_3]$, **10**, which can exist in two isomeric forms; *cis*- and *trans*-**10**, with C_3 and C_1 symmetry, respectively. While *cis*-**10** should display only a single resonance line for the *tert*-butyl protons, *trans*-**10** should give rise to three resonance lines of equal intensity, provided that the magnetic shift environments of the *tert*-butyl protons differ sufficiently. The exchange pattern(s) of the *tert*-butyl resonances provide information about the mechanism of inversion. A twist around the pseudo-C_3 axis of the *trans* isomer, for example, should result in a site exchange of two of the three *tert*-butyl resonances. This motion would not interchange the remaining *tert*-butyl signals of *cis*- and *trans*-**10**.

NMR Spectral Data for $H_2$9 and $K_3[Ga(9)_3]$, 10. As anticipated, **10** exists as an isomeric mixture of the two isomers *cis*-**10** and *trans*-**10**. However, at conditions where isomerization and inversion reactions for **4** are slow (i.e., in D_2O at 298 K), some of the resonance lines of **10** are exchange broadened and a discrete, static spectrum for the two isomers is obtained

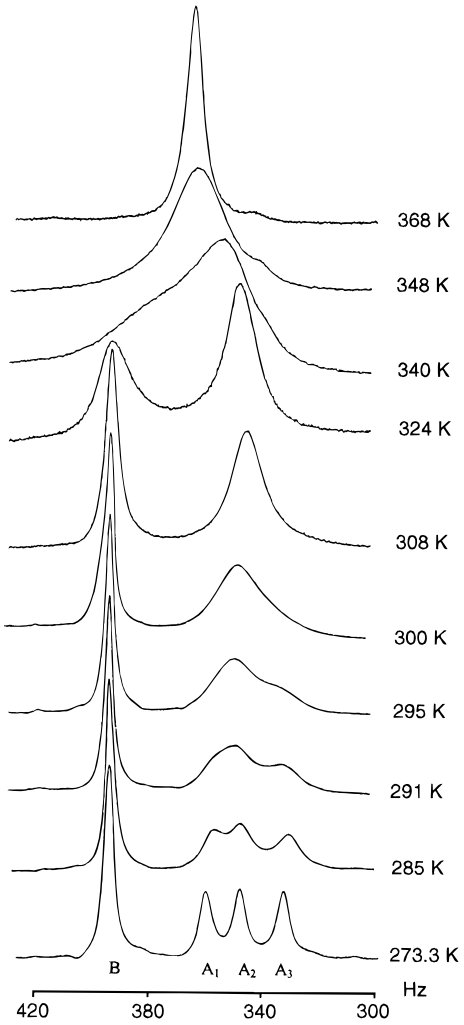

Figure 6. Variable temperature 300 MHz ^{1}H NMR spectra of the *tert*-butyl region of *cis*-**10** (B) and *trans*-**10** (A_1, A_2, A_3) in D_2O (pD 9.8). [**10**] = 0.015 M.

only at temperatures below 276 K and pD > 8 (see Figure 6, spectrum at 273 K); even under these conditions some of the resonances are significantly exchange broadened. Table 3 summarizes the observed resonances for H_2**9**, *cis*-**10**, and *trans*-**10** and their assignments. In D_2O, at 273 K the three resonances of equal intensity at 1.19, 1.15, and 1.10 ppm are assigned to the *tert*-butyl protons of the *trans* isomer (denoted A_1, A_2, and A_3 in Figure 6) while the resonance at 1.30 ppm is assigned to the *cis* isomer (B). From integration of the respective resonances, the ratio *cis*-**10**:*trans*-**10** in D_2O was determined to be 0.78(3), whereas a purely statistical isomer distribution would be 1/3. This value does not change in the temperature range 273−300 K, and yields $\Delta G°_{298} = 0.59(8)$ kJ mol^{-1} for the *cis* to *trans* equilibrium.[35] The ^{1}H NMR spectrum of **10** in DMSO-d_6 at 298 K displays only partially resolved *tert*-butyl proton resonances (see Figure 7). However, from their intensity ratios the resonances at 1.18 and 1.05 ppm (which has half the intensity of the resonance observed at 1.18 ppm) were readily assigned to the *trans* isomer, indicating that two of the three signals of *trans*-**10** are overlapping at 1.18 ppm (A_1, A_2). Again the equivalent *tert*-butyl protons of *cis*-**10** appear downfield from the resonances of *trans*-**10** at 1.26 ppm (B).

Intramolecular hydrogen bonding in both isomers results in a substantial downfield shift of both the $(CH_3)_3CNH$ and BzN*H* resonances; the absolute shift differences (∼2.7 and ∼1.9 ppm) are similar to those observed in **4** (∼2.15 ppm). The $(CH_3)_3$-CN*H* resonances were assigned to the *cis* and *trans* isomers from their intensity ratios. No assignments were made for the BzN*H* and the aromatic proton resonances.

The isomeric mixture of *cis*- and *trans*-**10** is expected to generate four AB patterns for the diastereotopic benzylic protons due to the chirality of the adjacent metal centers. $^3J_{H-H}$ coupling of the benzylic protons to BzN*H* in DMSO-d_6 solution required selective homonuclear decoupling to observe all eight spin doublets. After irradiation in the BzN*H* region all of the AB patterns were observed (see Figure 8). Although some of the resonance lines are overlapping, the single intense AB system can be readily assigned to the *cis* isomer (denoted C). The other three AB systems were assigned to the *trans* isomer (denoted T). The geminal coupling constant for all the benzylic protons of both isomers is 16 Hz. As pointed out earlier, in D_2O the *tert*-butyl resonances of *trans*-**10**, although resolved, are exchange broadened at 273.3 K, revealing that inversion is, to some extent, operative for the *trans* isomer at this temperature (*vide infra*). Accordingly the three AB systems of *trans*-**10** are exchange broadenend, and only the AB system of *cis*-**10** is observed.

Isomerization of *cis*- and *trans*-10. Figure 6 shows the variable temperature ^{1}H NMR spectrum of **10** in D_2O at pD 9.8, in the region of the *tert*-butyl resonances. At or just above ambient temperature one sharp (B) and one broadened signal are observed corresponding to *cis*-**10** and *trans*-**10**, respectively. As the temperature is raised this pattern passes through a coalescence point at $T_c = 340(1)$ K, and eventually resolves into a single resonance at 370 K. The collapse of *cis*- and *trans*-**10** *tert*-butyl signals is associated with the interconversion of both isomers. A control experiment, in which excess H_2**9** was added to the sample, showed no exchange broadening of the resonances due to the free ligand and the metal complexes, indicating that the mechanism of isomerization proceeds intramolecularly (Figure 9). At pD 12.1 the variable temperature ^{1}H NMR spectrum for **10** was unchanged. However, NMR spectra in the pD range 6−8 were markedly different, with patterns of the *tert*-butyl signals similar to those at elevated temperatures in the experiments performed at pD 9.8 and 12.1. Analysis of the variable temperature spectrum of **10** in DMSO-d_6 (Figure 7) produces a T_c of 360(1) K for the *cis*−*trans* isomerization. An increase of similar magnitude in T_c on changing the solvent to DMSO-d_6 was observed for inversion of **4**. Accordingly, the kinetic data reported herein support the proposal that this is due to the formation of contact ion pairs in DMSO-d_6 solution.

Inversion of *trans*-10 and *cis*-10. The process which can be clearly distinguished from *cis*−*trans* isomerization is inversion of *trans*-**10**. This can be seen from the exchange pattern of the *tert*-butyl resonances in the low-temperature region of the variable temperature spectrum of **10** in D_2O (Figure 6, 273−300 K) or DMSO-d_6 (Figure 7, 298−340 K). In D_2O, as the temperature is lowered below 300 K, the broadened pattern of *tert*-butyl resonances resolves into three single resonance lines (A_1−A_3) at 273.3 K. The 300 MHz ^{1}H NMR spectra (Figures 6 and 9) indicate that only two of the three signals (A_1 and A_3) are coalescing while the remaining signals of *trans*-**10** (A_2), *cis*-**10** (B), and ligand (C) are not affected. The coalescence temperature is 295(1) K with $\delta(A_1-A_3) = 27$ Hz at 273.3 K. Assuming that at this temperature exchange is slow, an approximate activation barrier for inversion of configuration of $\Delta G^{‡}_{295} \approx 60$ kJ mol^{-1} is calculated. A similar exchange pattern of *tert*-butyl resonances was observed in DMSO-d_6. Figure 7

(35) The *cis*-**10**:*trans*-**10** ratios in D_2O and DMSO-d_6 were found to be identical.

Table 3. ^{1}H NMR Data for H_2**9**, *cis*-K_3[Ga(**9**)$_3$], and *trans*-K_3[Ga(**9**)$_3$] in D_2O and DMSO-d_6

H_2**9**	*cis*-K_3[Ga(**9**)$_3$]		*trans*-K_3[Ga(**9**)$_3$]		
DMSO-d_6[a,c]	DMSO-d_6[a,c]	D_2O[b,c]	DMSO-d_6[a,c]	D_2O[b,c]	assignment
9.43 (t)	11.35−11.42 (m)	n.o.	11.35−11.42 (m)	n.o.	BzN*H*CO[d]
8.17 (s)	10.86 (s)	n.o.	10.91 (s)	n.o.	N*H*CO
			2 × 10.89 (s)	n.o.	
7.40−7.22 (m)	7.27−6.72 (m)	7.24−7.03 (m)	7.27−6.72 (m)	7.24−7.03 (m)	Ar*H*, Ar′*H*[d]
4.51 (d)	4.43 (d)	4.41 (d)	4.63 (d)	*e*	CH_2C$_6$H$_5$
	4.12 (d)	4.29 (d)	4.58 (d)	*e*	
			4.45 (d)	*e*	
			4.30 (d)	*e*	
			2 × 4.13 (d)	*e*	
1.39 (s)	1.26 (s)	1.30 (s)	2 × 1.18 (s)	1.19 (s)	C(CH_3)$_3$
			1.05 (s)	1.15 (s)	
				1.10 (s)	

[a] Chemical shifts are in ppm with respect to Me_4Si (0.0 ppm) at 298 K. [b] Chemical shifts are in ppm with respect to dioxane (3.75 ppm) at 273 K, pD 9.8. [c] Coupling constants are included in the Experimental Section; s = singlet, d = doublet, t = triplet, m = multiplet, n.o. = not observed. [d] The resonances in the range 7.5−7.0 ppm are unresolved at the spectrometer frequency used, but were assigned to the BzNH (Bz = benzyl) and aromatic protons (ArH and Ar′H denote the protons of the 2,3-dihydroxyterephthalamide ring and the protons of the phenyl ring, respectively) from their correct intensity ratio. [e] Resonances obscured by solvent resonances.

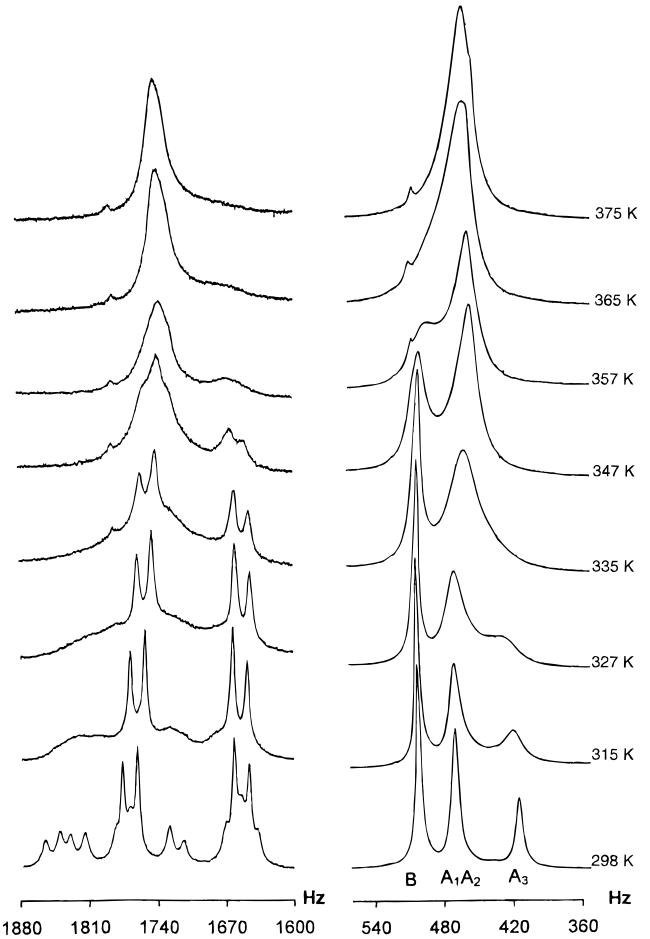

Figure 7. Variable temperature 400 MHz ^{1}H NMR spectra of the benzylic proton (left column) and 300 MHz ^{1}H NMR spectra of the *tert*-butyl proton region (right column) of a mixture of *trans*-**10**-d_6 (A_1, A_2, A_3), and *cis*-**10**-d_6 (B) in DMSO-d_6. [**10**] = 0.015 M. A deuterated sample was used to record the spectra in the benzylic proton region (see ref 36).

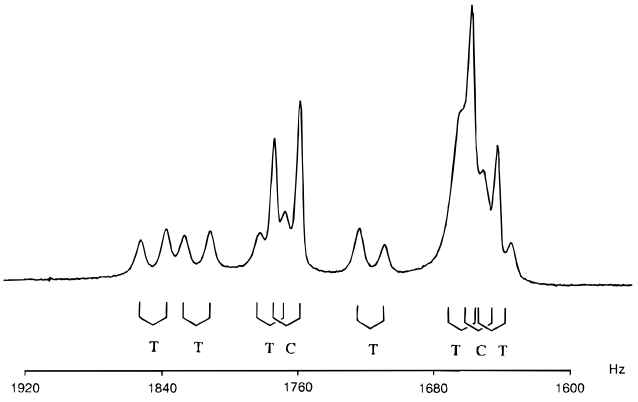

Figure 8. Experimental 400 MHz ^{1}H NMR spectrum of **10** (benzylic proton region) in DMSO-d_6 after irradiation in the benzyl proton region at 298 K. C and T denote the AB spin systems of *cis*-**10** and *trans*-**10**, respectively.

shows the variable temperature ^{1}H NMR spectrum of **10** in DMSO-d_6. The spectrum at 298 K reveals two *tert*-butyl signals with a 2:1 intensity ratio and a peak separation of 52 Hz for *trans*-**10** (A_1−A_3) and one singlet for *cis*-**10** (B). Upon raising the temperature, the signal at 420 Hz (A_3) coalesces with only one of the two chemical shift equivalent resonances at 472 Hz (A_1 or A_2) and both signals pass through a coalescence point at T_c = 327(1) K. The barrier to inversion of *trans*-**10** in DMSO-d_6 is estimated to be $\Delta G^{\ddagger} \approx 67$ kJ mol^{-1}. A similar increase in $\Delta G^{\ddagger}$ by ∼7 kJ mol^{-1} is obtained for the inversion of **4** when the solvent is changed from D_2O to DMSO-d_6. Again, *cis*−*trans* isomerization is slow up to temperatures as high as 335 K; however, line broadening of the *tert*-butyl resonance of *cis*-**10** at 335 K reveals some overlap of the two kinetic processes in the temperature range 335−345 K.

As shown in Figure 7, the temperature-dependent spectral changes in the benzylic proton region parallel the changes observed in the *tert*-butyl proton region. The three AB spin systems of *trans*-**10**-d_6[36] broaden and coalesce in the temperature range where inversion of *trans*-**10** was detected by the coalescence of the *tert*-butyl proton resonances. However, due to poorly resolved spin doublets and overlap with the resonances of *cis*-**10**-d_6, a discrete averaging pattern of the three AB systems was not seen. The two spin doublets of *cis*-**10**-d_6 start to broaden at ca. 335 K, revealing that the barrier to inversion for *cis*-**10** is larger than for *trans*-**10** (T_c = 327 K). Inversion of *cis*-**10** occurs in the same temperature interval as the process of *cis*−*trans* isomerization, and both result in complete averaging of all AB systems.

Mechanism of Inversion. The variable temperature ^{1}H NMR spectra of K_3[Ga(**9**)$_3$] in D_2O or DMSO-d_6 reveal two kinetic

(36) A deuterated sample was used to suppress $^3J_{HH}$ coupling to the amide proton. Deuteration of the amide groups in **10** was accomplished by repeated addition and evaporation of D_2O. The ^{1}H NMR spectra of **10** and **10**-d_6 in DMSO-d_6 are identical, except that the NH resonances are absent and the benzylic protons appear as an AB pattern for **10**-d_6.

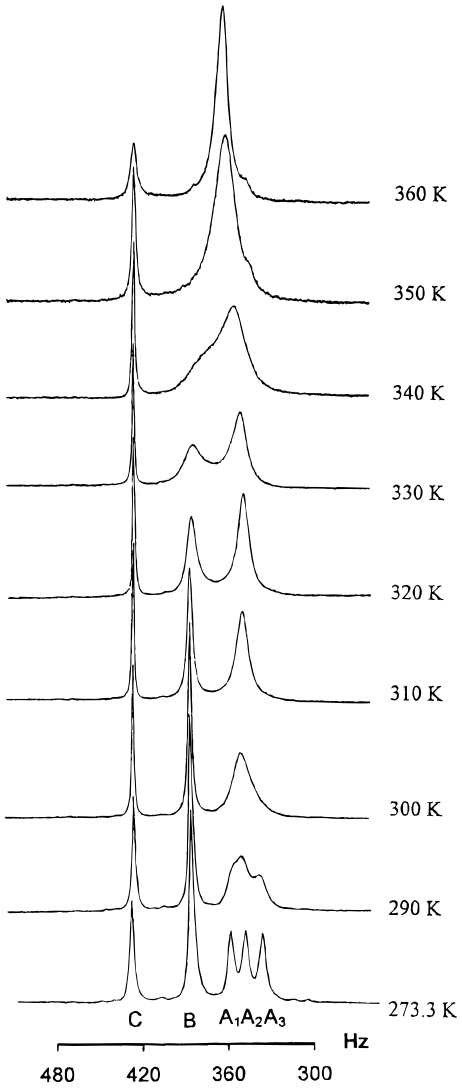

Figure 9. Variable temperature 300 MHz ^{1}H NMR spectra of the *tert*-butyl region of a mixture of *trans*-**10** (A_1, A_2, A_3), *cis*-**10** (B), and H_2**9** (C) in D_2O (pD 12.1). [**10**] = 0.015 M. [H_2**9**] = 0.008 M.

processes. In the lower part of the temperature range investigated, intramolecular rearrangement reactions are detected for the *trans*-**10** isomers. The spectral changes in the *tert*-butyl proton resonance region display an averaging of two of the three resonances of *trans*-**10**; the remaining resonances of *trans*-**10**, *cis*-**10**, or ligand, H_2**9**, are not affected. Inspection of the benzylic proton resonance region in this temperature interval clearly reveals that this motion involves inversion of configuration of *trans*-**10**. The other process is *cis*−*trans* isomerization, which starts to begin in a temperature range where inversion of *trans*-**10** is already fast and results in the collapse of all *tert*-butyl and benzylic proton resonances at higher temperatures.

Eaton *et al.*[22] have reported a permutational analysis of the averaging patterns expected for the different possible intramolecular rearrangement reactions of ML_3-type complexes (L = unsymmetrical chelate ligand). The observed two-site interchange in *trans*-**10**, involving inversion of configuration without isomerization, is fully consistent with only one of these sets, which corresponds to a trigonal twist mechanism about the pseudo 3-fold axes (Figure 10). *We therefore conclude that the mechanism of inversion of trans-**10** proceeds through a trigonal twist via a trigonal-prismatic transition state.* Compared to the *trans*-**10** isomers, the *cis*-**10** isomers are configurationally more rigid. This is indicated by the non-exchange-broadened AB system of the benzylic proton resonances of *cis*-**10** in the temperature range where inversion of *trans*-**10** is fast. However, mechanistic details of the inversion of the *cis* isomers could not be deduced from the variable temperature NMR spectra since *cis*−*trans* isomerization starts at higher temperatures. In the absence of *cis*−*trans* isomerization, a trigonal twist about the real C_3 axis of the *cis* isomer would result in pairwise averaging of the two spin doublets of the benzylic protons of *cis*-**10**. This would not affect the corresponding resonances of *trans*-**10**. Instead, *cis*−*trans* isomerization results in simultaneous averaging of all signals rather than discrete averaging of the respective resonances of *cis*-**10**.

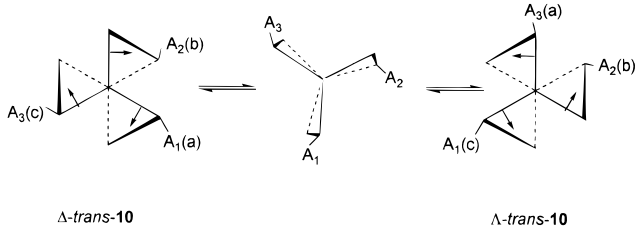

Figure 10. Inversion of configuration for *trans*-**10** by a trigonal twist about the pseudo-C_3 axis via an idealized trigonal prismatic transition state and corresponding site interchanges of *tert*-butyl groups in Δ- and Λ-*trans*-**10**. The inequivalent *tert*-butyl groups are denoted A_1, A_2, and A_3, and the inequivalent environments are denoted (a), (b), and (c).

The intramolecular rearrangement reactions of tricatecholatogallium(III) complexes we have identified are closely related to the rearrangement reactions of tristropolonato gallium(III) complexes.[23] The temperature dependent NMR spectra of tris(α-isopropenyltropolonato)- and tris(α-isopropyltropolonato)-gallium(III) complexes, for example, exhibit two similar separate kinetic processes in particular, overlapping temperature intervals. A trigonal twist mechanism has been established from the exchange pattern of methyl resonances for the *trans* isomers in the low-temperature region, while at elevated temperatures *cis*−*trans* isomerization occurs. The coalescence temperatures and free energy barriers to inversion for the tritropolonatogallium(III) complexes are $T_c = -65$ °C and $\Delta G^{\ddagger} = 40$ kJ mol^{-1}. For the tricatecholatogallium(III) complexes described in this paper the free energy barrier to inversion is $\Delta G^{\ddagger} = 60$ kJ mol^{-1}; the tropolonates invert much faster than the catecholates.

Conclusions

Inversion and isomerization reactions have been characterized for triscatecholato complexes of gallium(III). Compared to tropolonates, the catecholate complexes invert much slower, consistent with their greater thermodynamic stability. The rate of inversion of the $[Ga(L)_3]^{3-}$ complexes (L = 2,3-dihydroxy-*N*,*N*′-substituted-terephthalamide) is pH independent above pH 9 and proceeds by an intramolecular mechanism. Below this pH the rate of inversion is first order with respect to $[H^+]$, with this pathway rapidly becoming dominant. This enhancement in the rate of inversion is due to the formation of a monoprotonated complex $H[GaL_3]^{2-}$. The mechanism of inversion of the $[GaL_3]^{3-}$ complex has been elucidated from the independent site interchange of *tert*-butyl resonances in *trans*-**10**, which is consistent with only one model: a trigonal twist around the pseudo-C_3 axis, resulting in a trigonal-prismatic transition state. *Cis*−*trans* isomerization also proceeds intramolecularly with a larger activation barrier. Isomerization and inversion reactions of $[GaL_3]^{3-}$ anions (with L = bidentate 2,3-dihydroxyterephthalamide chelating units similar to the catechol amide chelating units found in enterobactin, and gallium(III) as an appropriate structural and rate simulator for Fe(III)) are fast on the NMR time scale, in particular in the pH region close to *in-vivo* pH

values. A function of the cyclic triserine backbone of enterobactin is to fix the *cis*-Δ-configuration at the metal center. The relatively rapid rate of isomerization seen in the model complexes indicates that the inversion rate of the metal center in the ferric complex of enterobactin is probably rapid on the time scale of microbial iron transport. Hence, the observed chiral specificity of iron delivery is a thermodynamic, not kinetic, property of the siderophore.

Experimental Section

Physical Measurements. The ^{1}H NMR and ^{13}C NMR spectra were obtained on either a Bruker AMX 300 or AMX 400 spectrometer. Absorption spectra were recorded on an HP 8452A vis/UV diode array spectrophotometer. Concentrations of the solutions were analyzed for iron by atomic absorption. The extinction coefficients for the spectra are based on these concentrations. Infrared spectra were measured as KBr pellets using a Nicolet Magna IR 550 spectrometer. Melting points were taken on a Büchi melting apparatus and are uncorrected. Microanalyses were performed by the Analytical Services Laboratory, College of Chemistry, University of California, Berkeley. Fast-atom-bombardment mass spectra were obtained at the Mass Spectrometry Laboratory at the University of California, Berkeley.

Variable Temperature ^{1}H NMR Measurements. Variable temperature experiments were carried out on a Bruker AMX 300 spectrometer operating at 300 MHz. The temperature was controlled by the B-VT2000 equipment of the spectrometer that ensures a precision of ±1 °C. The probe temperature was allowed to equilibrate for 10 min prior to final magnetic homogeneity optimization on the ^{1}H FID. Variation at a given temperature was less than ±0.1 °C. For each sample the temperature was varied in both directions, and in each case superimposable spectra were obtained. The samples were prepared by adding the pure metal complexes to buffered D_2O solutions (5% KH_2PO_4). Final sample concentrations were approximately 0.015 M. After sample preparations, pD values were adjusted with D_2O solutions of 10% NaOD and determined by use of a Fisher Accumet digital pH meter fitted with a glass electrode (pD = pH meter reading + 0.4).[37] The electrode was calibrated with standard commercial buffers of pH 4.00 and 10.00. All chemical shifts were referenced to dioxane as an internal standard.

The temperature behavior of the methyl proton resonances for **4** was investigated in D_2O at different pD values over the range 275−360 K. The kinetic parameters for the inversion of **4** were determined by lineshape analysis.[38] The experimental spectra were simulated as a two-site exchange process using the program DNMR3.[39] Line widths (2.40 Hz), coupling constants ($^3J_{HH}$ = 6.52 Hz, $^4J_{HH}$ = 0.0 Hz), and relative intensities (0.5, 0.5) for both methyl proton resonances at slow exchange were obtained at 273.3(1) K, pD 12.10, and used as fixed parameters in the calculations. The separation between the signals at temperatures at or above coalescence temperature were obtained from an extrapolation of the shift differences in the temperature range 273.3−310 K. Rate constants for each temperature were determined by comparison of the calculated and experimental spectra.

Proton NMR spectra of the gallium complex $K_3[Ga(\mathbf{3})]_3$ were obtained in buffered $KH_2PO_4/KHPO_4$ D_2O solutions (pD range 6.2−9.0). Samples were prepared as indicated above. Data were collected on a Bruker AMX 300 spectrometer at 295 K. Rate constants for each pD value were determined as described above.

Potentiometric Titrations. Solution thermodynamic data were obtained by potentiometric pH titrations. Ligand protonation constants for several 2,3-dihydroxy-*N*,*N*′-disubstituted-terephthalamides are literature values.[31] For $H_2\mathbf{3}$, the protonation constants were estimated to be log K_{011} = 11.1 and log K_{012} = 6.0.[31] Complex protonation constants were determined potentiometrically in a 0.1 M KCl solution at 25.0 °C with a Dosimat automatic titration system using a calibrated KCl glass electrode.[40] Solutions were titrated with degassed, standardized 0.1 M KOH and 0.1 M HCl under argon. Solutions (50 mL, approximately 0.05 mmol of the compounds) were titrated both from base to acid (pH range 4−11.2) and vice versa, to check for hysteresis. The complex protonation constants were modeled with a version of the program BETA90, described elsewhere.[41]

Preparation of Compounds.[42] Unless otherwise noted, all starting materials were obtained commercially and used without further purification. 3,3′-(2,3-Dimethoxyterephthaloyl)bis(1,3-thiazolidine-2-thione),[43] **1**, and sodium methyl-2,3-dimethoxyterephthalate,[44] **6**, were synthesized according to literature procedures. Silica gel 60 (Merck, 230−400 mesh) was used for column chromatography. Organic solvents and mineral acids were of reagent grade; tetrahydrofuran (THF) was distilled from sodium benzophenone ketyl prior to use. Water was deionized, and further purified by a Millipore cartridge system (resistivity 18 MΩ cm). Metal complex syntheses were performed under an argon atmosphere using Schlenk techniques.

(I) Ligand Syntheses. 2,3-Dimethoxy-*N*,*N*′-diisopropylterephthalamide (2). Compound **1** (4.29 g, 10 mmol) was dissolved in 100 mL of CH_2Cl_2 and was added to a stirred solution of isopropylamine (2.60 mL, 30.3 mmol) dissolved in 100 mL of CH_2Cl_2. After stirring for 2 h, the volatiles were removed *in vacuo*, leaving a pale yellow residue. The residue was redissolved in 250 mL of CH_2Cl_2, washed three times with 1 M KOH, dried over anhydrous $MgSO_4$, and filtered. Removal of the solvent afforded a white residue which was recystallized from CH_3OH/H_2O. Yield: 2.93 g (94%). ^{1}H NMR (300 MHz, $CDCl_3$): δ 7.89 (s, 2H, Ar*H*), 7.64 (d, *J* = 6.8 Hz, 2H, CON*H*), 4.29 (oct, *J* = 6.8 Hz, 2H, C*H*), 3.92 (s, 6H, OCH_3), 1.27 (d, *J* = 6.6 Hz, 12H, CH_3). ^{13}C{^{1}H} NMR (100 MHz, $CDCl_3$): δ 22.4, 41.1, 61.1, 125.7, 129.9, 151.0, 162.9. Anal. Calcd (Found) for $C_{16}H_{24}O_4N_2$: C, 62.32 (62.00); H, 7.84 (7.94); N, 9.08 (9.03).

2,3-Dihydroxy-*NN*′-diisopropylterephthalamide ($H_2$3). Compound **2** (2.90 g, 9.40 mmol) was dissolved in 100 mL of CH_2Cl_2. BBr_3 (7 mL, 73 mmol) was added *via* syringe, and the slurry was stirred for 12 h. The cloudy, pale yellow mixture turned clear upon the addition of 50 mL of methanol. Repeated addition of methanol (16 × 50 mL) followed by evaporation afforded a pale yellow solid. The solid was dissolved in 20 mL of CH_3OH, and precipitation with water afforded white crystals. Mp: 240 °C. Yield: 1.89 g (72%). FT-IR (KBr, cm^{-1}): $\bar{\nu}$ 3421, 3371 (NH), 1597, 1537 (CO). ^{1}H NMR (300 MHz, DMSO-d_6): δ 8.60 (d, *J* = 7.7 Hz, 2H, N*H*CO), 7.35 (s, 2H, Ar*H*), 4.14 (oct, *J* = 6.8 Hz, 2H, C*H*), 1.18 (d, *J* = 6.6 Hz, 12H, CH_3). ^{13}C{^{1}H} NMR (100 MHz, CD_3OD): δ 22.5, 42.9, 117.7, 119.5, 150.2, 169.1. Anal. Calcd (Found) for $C_{14}H_{20}O_4N_2$: C, 59.99 (59.62); H, 7.19 (7.16); N, 9.99 (9.92).

2,3-Dimethoxy-4-(*tert*-butylcarbamoyl)benzoic acid (7). Compound **6** (3.14 g, 12 mmol) was added in portions to 16 mL of freshly distilled $SOCl_2$ (at 0 °C) and stirred for 12 h at 25 °C. The pale yellow solution was filtered to remove solid NaCl. Coevaporation of the solution *in vacuo* with CCl_4 (3 × 30 mL) afforded the acid chloride which was used without further purification. The acid chloride was dissolved in 70 mL of dry THF, and a solution of *tert*-butylamine (1.25 mL, 12.2 mmol) and triethylamine (1.3 mL) in 70 mL of THF was added at 0 °C. The reaction mixture was stirred for 1 h, during which time the solution turned yellow, with formation of solid $Et_3N{\cdot}HCl$. After filtration and removal of the solvent on a rotary evaporator, the residue was taken up in 300 mL of CH_2Cl_2 and washed three times with 50 mL of 0.2 M HCl. Removal of the solvent by rotary evaporation afforded a pale yellow solid. The solid was dissolved in 30 mL of CH_3OH, and 30 mL of 4 M NaOH was added. After 1 h, the solution was brought to pH 2 with HCl (6 M) and the acid was extracted with

(37) Glasoe, P. K.; Long, F. A. *J. Phys. Chem.* **1960**, *64*, 188.

(38) *Dynamic Nuclear Magnetic Resonance Spectroscopy*; Jackman, L. M., Cotton, F. A., Eds.; Academic Press: New York, 1975.

(39) Binsch, G.; Kleier, D. *Quantum Chemistry Program Exchange*, No. 165. DNMR3 is part of The University of Manitoba NMR Spectral Simulation and Analysis Package. X-11/Motif Version 940101.

(40) (a) Scarrow, R. D. Ph.D. Dissertation, University of California at Berkeley, 1985. (b) Turowski, P. N.; Rodgers, S. J.; Scarrow, R. C.; Raymond, K. N. *Inorg. Chem.* **1988**, *27*, 474.

(41) Franczyk, T. S. Ph.D. Dissertation, University of California at Berkeley, 1991.

(42) Abbreviations: acac, 2,4-pentanedione; DCC, 1,3-dicyclohexylcarbodiimide; DCU, 1,3-dicyclohexylurea; DMAP, 4-(dimethylamino)pyridine; NBA, *p*-nitrobenzyl alcohol; TGG, thioglycerol/glycerol.

(43) Karpishin, T. B.; Stack, T. D. P.; Raymond, K. N. *J. Am. Chem. Soc.* **1993**, *115*, 182.

(44) Weitl, F. L.; Raymond, K. N.; Durbin, P. W. *J. Med. Chem.* **1981**, *24*, 203.

diethyl ether (three times). The combined ether extracts were dried over anhydrous $MgSO_4$ and filtrated, and the solvent was removed to afford a pale yellow solid which was used without further purification in the next reaction. Yield: 3.20 g (95%). ^{1}H NMR (300 MHz, DMSO-d_6): δ 7.94 (s, 1H, N*H*), 7.38, 7.23 (2d, J = 8.1 Hz, 1H each, Ar*H*), 3.82 (s, 3H, OCH_3), 3.81 (s, 3H, OCH_3), 1.35 (s, 9H, C(CH_3)$_3$).

2,3-Dimethoxy-*N*-butyl-*N*′-benzylterephthalamide (8). Compound **7** (3.20 g, 11 mmol), DCC (2.5 g, 12 mmol), and catalytic DMAP (13 mg) were dissolved in 25 mL of CH_2Cl_2. After 20 min of stirring, benzylamine (1.2 mL, 11 mmol) was added and a white precipitate formed. The reaction mixture was stirred for 2 days, and insoluble DCU was removed by filtration. The pale yellow oil which was obtained after rotary evaporation was applied to a silica gel column and eluted with ethyl acetate/hexanes (v/v = 0.6, R_f = 0.26) and used without further purification in the next reaction. Yield: 2.6 g (64%). ^{1}H NMR (300 MHz, DMSO-d_6): δ 8.78 (t, J = 7.7 Hz, 1H, N*H*), 7.93 (s, 1H, N*H*), 7.35 - 7.21 (m, 5H + 2H, Ar*H*), 4.47 (d, J = 7.7 Hz, 2H, CH_2), 3.83 (s, 3H, OCH_3), 3.80 (s, 3H, OCH_3), 1.36 (s, 9H, C(CH_3)$_3$).

2,3-Dihydroxy-*N*-butyl-*N*′-benzylterephthalamide ($H_2$9). Compound **8** (2.6 g, 7 mmol) was dissolved in 80 mL of CH_2Cl_2. BBr_3 (4.7 mL, 49 mmol) was added carefully *via* syringe, and the slurry was stirred for 12 h. The cloudy, pale yellow mixture turned clear upon the addition of 50 mL of methanol. Repeated addition of methanol (16 × 50 mL) followed by evaporation afforded a pale yellow solid. The solid was dissolved in methanol (20 mL) and precipitated with water to obtain white crystals. Mp: 173 °C. Yield: 1.80 g (75%). FT-IR (KBr, cm^{-1}) $\bar{\nu}$ 3393, 3337 (NH), 1598, 1535 (CO). ^{1}H NMR (300 MHz, DMSO-d_6): δ 9.43 (t, J = 6.0 Hz, 1H, N*H*), 8.17 (s, 1H, N*H*), 7.40−7.22 (m, 5H + 2H, Ar*H*), 4.51 (d, J = 6.0 Hz, 2H, CH_2), 1.39 (s, 9H, C(CH_3)$_3$). ^{13}C{^{1}H} NMR (100 MHz, D_2O/NaOD): δ 29.7, 44.0, 51.3, 112.9, 113.0, 117.6, 119.4, 128.4, 130.0, 140.3, 165.3, 166.0, 173.1. Anal. Calcd (Found) for $C_{19}H_{22}O_4N_2$: C, 66.65 (66.33); H, 6.48 (6.53); N, 8.18 (8.12).

(II) Metal Complex Syntheses. K_3[Ga(3)$_3$] (4). To H_2**3** (134 mg, 0.48 mmol) dissolved in MeOH were added a solution of KOH in EtOH (0.5 M, 1 mL) and solid Ga(acac)$_3$ (60 mg, 0.16 mmol). After the solution was stirred for 30 min the volatiles were removed *in vacuo*, leaving a pale yellow solid. The solid was recrystallized from acetonitrile, filtrated, and air-dried. Yield: 141 mg (86%). FT-IR (KBr, cm^{-1}) $\bar{\nu}$ 3439, 3207 (NH), 1610, 1563 (CO). ^{1}H NMR (300 MHz, DMSO-d_6): δ 10.76 (d, J = 6.6 Hz, 6H, N*H*CO), 6.65 (s, 6H, Ar*H*), 3.84 (oct, J = 6.6 Hz, 6H, C*H*), 1.09 (d, J = 6.6 Hz, 18H, CH_3), 0.95 (d, J = 6.6 Hz, 18H, CH_3). ^{13}C{^{1}H} NMR (100 MHz, CD_3OD): δ 23.0, 23.4, 42.1, 113.7, 116.3, 159.8, 170.7. +FAB-MS (TGG): *m*/*e* 1022 [M + H]$^+$, 983 [M + 2H − K]$^+$, 946 [M + 3H − 2K]$^+$. Anal. Calcd (Found) for $K_3GaC_{42}H_{54}O_{12}N_6$·($H_2O$)$_{12}$: C, 41.35 (41.79); H, 6.28 (5.99); N, 6.89 (6.74).

K_3[Fe(3)$_3$] (5). Compound **5** was prepared by the procedure detailed above for **4** using Fe(acac)$_3$ (56 mg, 0.16 mmol) instead of Ga(acac)$_3$. Yield: 145 mg (89%). FT-IR (KBr, cm^{-1}) $\bar{\nu}$ 3408, 3230 (NH), 1605, 1565 (CO). Vis/UV spectrum (H_2O, 5% K_2HPO_4): λ_{max} = 364 nm (ϵ = 10 500 M^{-1} cm^{-1}), 446 nm (ϵ = 5200 M^{-1} cm^{-1}), 512 nm (ϵ = 4500 M^{-1} cm^{-1}). +FAB-MS (CH_3OH/NBA): *m*/*e* 1008 [M + H]$^+$, 970 [M + 2H − K]$^+$, 932 [M + 3H − 2H]$^+$. Anal. Calcd (Found) for $K_3FeC_{42}H_{54}O_{12}N_6$·($H_2O$)$_8$: C, 43.78 (43.53); H, 6.12 (5.88); N, 7.29 (7.89).

K_3[Ga(9)$_3$] (10). Compound **10** was prepared by the procedure detailed above for **4**. H_2**9** (170 mg, 0.50 mmol) was used instead of H_2**3**. Yield: 179 mg (93%), pale yellow solid. FT-IR (KBR, cm^{-1}) $\bar{\nu}$ 3411, 3228 (NH), 1628, 1560 (CO). ^{1}H NMR (400 MHz, DMSO-d_6): δ 11.41 (m, 3H, N*H*CH$_2$), 10.91, 10.89, 10.86 (3 s, 3H, N*H*), 7.26−6.72 (m, 15H + 6H, Ar*H*), 4.67−4.08 (m, 6H, CH_2), 1.26, 1.18, 1.05 (3 s, 9H, C(CH_3)$_3$). +FAB-MS (CH_3OH/NBA): *m*/*e* 1208 [M]$^+$, 1247 [M + K]$^+$. Anal. Calcd (Found) for $K_3GaC_{57}H_{60}O_{12}N_6$·($CH_3CN$)($H_2O$)$_3$: C, 54.38 (54.44); H, 5.34 (5.24); N, 7.52 (7.72).

K_3[Fe(9)$_3$] (11). Compound **11** was prepared by the procedure detailed above for **5**. H_2**9** (170 mg, 0.50 mmol) was used instead of H_2**3** and Fe(acac)$_3$ instead of Ga(acac)$_3$. Yield: 164 mg (83%). UV/vis spectrum (H_2O, 5% K_2HPO_4) λ_{max} = 364 nm (ϵ = 10 400 M^{-1} cm^{-1}), 448 nm (ϵ = 5500 M^{-1} cm^{-1}), 516 nm (ϵ = 4800 M^{-1} cm^{-1}). +FAB-MS (NBA) *m*/*e* 1194 [M + H]$^+$. Anal. Calcd (Found) for $K_3FeC_{57}H_{60}O_{12}N_6$·($H_2O$)$_5$ C, 53.31 (53.28); H, 5.49 (5.49); N, 6.54 (6.25).

[NMe$_4$]$_3$[Ga(3)$_3$] (12). H_2**3** (134 mg, 0.48 mmol) and NMe_4OH·5H_2O (87 mg, 0.48 mmol) were dissolved in 5 mL of CH_3OH. Ga(acac)$_3$ (59 mg, 0.16 mmol) was added, and the solution was stirred for 30 min. **12** was precipitated by addition of diethyl ether, recrystallized from 2-propanol, and air-dried. Yield: 143 mg (80%), colorless crystals. FT-IR (KBr, cm^{-1}) $\bar{\nu}$ 1627, 1545 (CO). ^{1}H NMR (300 MHz, CD_3OD): δ 6.96 (s, 6H, Ar*H*), 4.03 (spt, 6H, C*H*), 2.94 (s, 36H, N(CH_3)$_4^+$), 1.22 (d, 18H, CH(CH_3)$_2$), 1.04 (d, 18H, CH(CH_3)$_2$). ^{13}C{^{1}H} NMR (100 MHz, CD_3OD): δ 23.2, 23.7, 42.2, 55.7, 113.4, 115.8, 160.2, 170.7. +FAB-MS (NBA): *m*/*e* 1126 [M]$^+$, 1127 [M + H]$^+$, 1200 [M + NMe$_4$]$^+$. Anal. Calcd (Found) for $C_{54}H_{90}O_{12}N_9Ga$•(H_2O)$_3$: C, 55.34 (55.58); H 8.62 (8.88); N 8.77 (9.26).

[NMe$_4$]$_3$[Fe(3)$_3$] (13). Compound **13** was prepared by the procedure detailed above for **12**. Fe(acac)$_3$ was used instead of Ga(acac)$_3$. The red crystals obtained were dried at 30 °C *in vacuo* overnight. Yield: 144 mg (76%). FT-IR (KBr, cm^{-1}) $\bar{\nu}$ 1617, 1557 (CO). Vis/UV spectrum (H_2O, 5% K_2HPO_4): λ_{max} 364 nm (ϵ = 12 000 M^{-1} cm^{-1}), 448 nm (ϵ = 6700 M^{-1} cm^{-1}), 512 nm (ϵ = 5800 M^{-1} cm^{-1}). +FAB-MS (TGG): *m*/*e* 1114 [M + H]$^+$, 1187 [M + NMe$_4$]$^+$. Anal. Calcd (Found) for $C_{54}H_{90}O_{12}N_9Fe$·H_2O: C, 57.34 (57.09); H 8.20 (7.96); N 11.14 (11.07).

Acknowledgment. This work was supported by NIH Grants AI11744 and DK32999. B.K. thanks the Deutsche Forschungsgemeinschaft for a postdoctoral fellowship. We thank Professor R. C. Fay for helpful comments.

Supporting Information Available: Arrhenius plots of DNMR3 kinetic data from complete line-shape analysis of ^{1}H NMR spectra for **4** (1 page). Ordering information is given on any current masthead page.

JA953545F